JGR Earth Surface

RESEARCH ARTICLE
10.1029/2019JF005440

Revised Estimates of Recent Mass Loss Rates for Penny Ice Cap, Baffin Island, Based on 2005–2014 Elevation Changes Modified for Firn Densification

N. Schaffer[1,2], L. Copland[1], C. Zdanowicz[3], D. Burgess[4], and J. Nilsson[5]

[1]Department of Geography, Environment and Geomatics, University of Ottawa, Ottawa, Ontario, Canada, [2]Centro de Estudios Avanzados en Zonas Áridas (CEAZA), Universidad de La Serena, IV Región, La Serena, Chile, [3]Department of Earth Sciences, Uppsala University, Uppsala, Sweden, [4]Natural Resources Canada, Geological Survey of Canada, Ottawa, Ontario, Canada, [5]Jet Propulsion Laboratory, NASA, California Institute of Technology, Pasadena, CA, USA

Key Points:
- We report updated elevation changes for Penny Ice Cap, modified for firn densification to isolate surface mass change
- Accounting for firn densification reduces the inferred ice-cap-wide surface mass loss by ~13–15%
- There has been a fourfold increase in mass loss from Penny Ice Cap between 1995–2000 and 2005–2013

Supporting Information:
- Supporting Information S1

Correspondence to:
N. Schaffer,
nicole.schaffer@gmail.com

Citation:
Schaffer, N., Copland, L., Zdanowicz, C., Burgess, D., & Nilsson, J. (2020). Revised estimates of recent mass loss rates for Penny Ice Cap, Baffin Island, based on 2005–2014 elevation changes modified for firn densification. *Journal of Geophysical Research: Earth Surface*, *124*, e2019JF005440. https://doi.org/10.1029/2019JF005440

Received 9 NOV 2019
Accepted 4 MAY 2020

Abstract Repeat airborne or satellite measurements of surface elevation over ice caps are often used to calculate glacier-wide surface mass changes over time. However, these measurements typically do not account for vertical ice motion caused by firn densification and/or ice flow, so the effect of these factors for mass change measurements over an entire ice cap are currently poorly constrained. In this study, we update NASA Airborne Topographic Mapper (ATM) altimetry elevation changes across Penny Ice Cap (Baffin Island, Canada) to assess total changes in ice mass from 2005–2014, relative to 1995–2000. Dual-frequency GPS measurements and temporal changes in ice core density profiles are used to calculate firn densification and ice flow to isolate the component of elevation change due to surface mass change. Envisat satellite imagery is used to delineate the areas impacted by firn densification. These calculations, the first for a Canadian Arctic ice cap, indicate that accounting for firn densification may reduce the inferred surface mass loss by ~13–15%. Overall, there has been a fourfold increase in mass loss from Penny Ice Cap between 1995–2000 (-1.3 ± 0.7 Gt a^{-1}) and 2005–2013 (-5.4 ± 1.9 Gt a^{-1}). The rapid upglacier migration of the equilibrium line has left large areas of subsurface firn in the current ablation area and has far outpaced the ice flow response, illustrating that the ice cap is not in equilibrium and out of balance with the current climate.

1. Introduction

Glaciers of the Canadian Arctic Archipelago (CAA) have experienced increasing rates of mass loss in recent decades, particularly since 2005 (Gardner et al., 2011; Harig & Simons, 2016; Millan et al., 2017; Noël et al., 2018). As a result, glaciers in this region are now the largest contributors to eustatic sea level rise outside of Greenland, Antarctica, and Alaska (Box et al., 2018; Gardner et al., 2011; Jacob et al., 2012). The southern part of the CAA (Baffin and Bylot Islands) has lost ice mass at an area-averaged rate that is at least 1.6 times greater than the northern CAA since 1996 (Gardner et al., 2012; Noël et al., 2018). Air temperatures have increased throughout the southern Canadian Arctic since 1948, with the largest warming occurring in the winter months (Vincent et al., 2015), and glacier mass losses have been shown to correlate with rising summer temperatures (Gardner et al., 2011; Sharp et al., 2011). Projections by a coupled atmosphere/snow model forced with the Intergovernmental Panel on Climate Change's (IPCC) moderate RCP4.5 greenhouse gas emission scenario forecasts sustained and irreversible glacier mass losses in the CAA, increasing from -51 ± 26 Gt a^{-1} over 2000–2011 to -144 ± 33 Gt a^{-1} by the end of the 21st century, resulting in a projected 18% loss of the current ice volume (Lenaerts et al., 2013).

Repeat airborne measurements of elevation change have been widely used to quantify the response of glaciers and ice caps to climate warming over the past few decades (e.g., Abdalati et al., 2004; Gardner et al., 2011, 2012). Typically, in such studies, the observed surface elevation change of a glacier or ice cap over a given time interval (dh/dt) is used to directly calculate its mean surface mass loss or gain over the period between repeat altimetry surveys ($\dot{b}$). The term $\dot{b}$ is often referred to as mass balance rate (Cogley et al., 2011). However, there can be a change in surface elevation at a point on a glacier due to a change in firn densification rate or ice flow without actual mass loss. For example, on Devon Ice Cap (northern CAA), the near-surface firn density was found to have increased by 13–80% between 2005 and 2012,

corresponding to a surface lowering rate of 0.02–0.17 m a^{-1}, which accounts for the majority of measured elevation change above 1,650 m a.s.l. (above sea level; Bezeau et al., 2013). At the summit of Penny Ice Cap (hereafter: PIC) on southern Baffin Island, the firn density has also increased due to the formation of refrozen meltwater layers, resulting in a 6% increase in cumulative ice-equivalent thickness between 1995 and 2010 (Zdanowicz et al., 2012).

Several studies have sought to model firn densification and/or dynamic compaction in order to quantify their contribution to *dh/dt* in the dry snow zones of Greenland and Antarctica and on Greenland's glaciers and ice caps (Bolch et al., 2013; Cuffey, 2001; Gardner et al., 2013; Gascon et al., 2013; Li et al., 2003; Ligtenberg et al., 2015, 2018; Morris & Wingham, 2014; Shepherd et al., 2012; Zwally & Li, 2002). A simpler approach, used in other studies, is to apply a bulk density value less than 917 kg m^{-3} when converting geodetic volume changes to mass changes (Berthier et al., 2014; Huss, 2013; Thomson et al., 2017). We define the geodetic method as repeat measurements of surface elevation. Gardner et al. (2012) accounted for variations in firn density when quantifying uncertainties on geodetic estimates of mass changes for glaciers in the southern CAA (Table S1 in the supporting information). However, at present, no studies of CAA glaciers have attempted to use in situ data to quantify the contribution of firn densification to geodetic mass balance changes.

The present study focuses on PIC, which is the largest ice mass in the southern CAA (Figure 1). In previous studies, changes in *dh/dt* over PIC were estimated from NASA Airborne Topographic Mapper (ATM) laser altimetry data (hereafter: altimetry) between 1995 and 2005, ICESat satellite altimetry data between 2003 and 2009, and comparison of digital elevation models (DEMs) at lower elevations on the ice cap between 1958 and 2009 (Abdalati et al., 2004; Gardner et al., 2011, 2012). Since 2005, there have been additional altimetry surveys over PIC including in 2013 and 2014 (Figure 1). Using these new data, we update estimates of *dh/dt* over PIC to 2014 and use in situ measurements of elevation change (2011–2014), surface mass change (2006–2014), and data from firn/ice cores to account for the effects of vertical motion due to ice flow and changing firn densification rates.

2. Study Site

At 67°N, PIC is the southernmost large Canadian Arctic ice cap, covering an area of ~6,300 km^2 (Figure 1). The ice cap rises to ~1,930 m a.s.l., and major outlet glaciers flow from its interior down deeply incised valleys toward the north, east, and south. Higher topography and relief dominate the eastern side of the ice cap, trending toward lower elevations to the west where PIC terminates in a broad, gently sloping lobe-like region. The highest surface velocities on the ice cap occur on the outlet glaciers in areas of high relief, with rates of ~100–120 m a^{-1}, while the interior and the western sectors are generally slow moving at <40 m a^{-1} (Schaffer et al., 2017; Van Wychen et al., 2015). In contrast to Barnes Ice Cap (central Baffin Island) and Bylot Island Ice Cap, none of the outlet glaciers on PIC appear to be surge type (Van Wychen et al., 2015). There are two tidewater terminating glaciers on PIC: Coronation Glacier in the southeast sector and an unnamed glacier in the north-central sector. These glaciers discharge ~11 and ~9 Mt a^{-1}, respectively, which accounted for 0.2% of the total mass loss (by melting and calving) over PIC in 2011 (Van Wychen et al., 2015). The mean, maximum, and minimum annual air temperatures measured at the summit of PIC between 1 August 2007 and 31 July 2008 were −15.4°C, 2.9°C, and −42.9°C, respectively (Schaffer, 2019; Zdanowicz et al., 2012). The average dates for the onset and end of the summer melt period, as determined from spaceborne passive microwave measurements, were ~23 May and ~3 September, respectively, over the period 2007–2010 (F. Dupont, personal communication, 2015).

Annual measurements of surface mass loss or gain ($\dot{b}_{insitu}$) have been conducted on PIC since 2006 along three survey lines (designated 100, 200, and 300; Figure 1; Schaffer, 2019). These measurements were taken in the spring each year (usually April). In this paper, we describe $\dot{b}_{insitu}$ measurements in relation to the measurement year (e.g., April 2013–2014) which is the same year and includes the same summer season (e.g., 2013) as the geodetic year. In contrast, the mass balance year that corresponds to the same summer (e.g., 2013) would be the preceding year (e.g., 2012–2013), as this yearly cycle begins at the start of the accumulation season (e.g., September). Therefore, the mass loss rates reported for 2005–2013 in this paper refer to geodetic years and include field measurements up to April 2014.

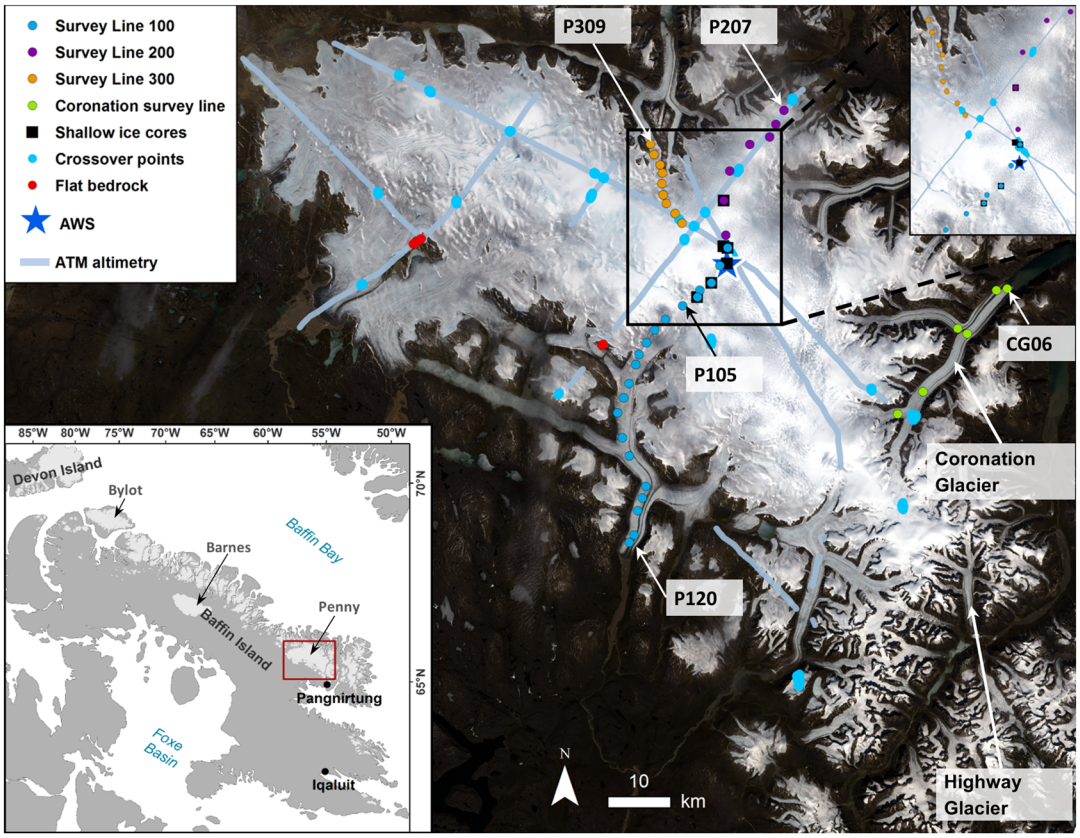

Figure 1. Map of Penny Ice Cap (67°N, 66°W) with mass balance survey lines, location of shallow ice cores, automatic weather station (AWS), altimetry flight lines, 2013 altimetry crossover points, and geodetic control points over flat bedrock. Crossover points outside the glacier boundary were excluded from the error analysis. The inset map identifies the location of Penny Ice Cap (red box), Barnes Ice Cap, and Bylot Island Ice Cap. Background image: Landsat 8, 21 July 2015.

Based on $\dot{b}_{insitu}$ measurements, the mean equilibrium line altitude (ELA) measured between 2006 and 2014 was ~1,646 m a.s.l., varying between ~1,320 m in low mass loss years and ~1,820 m during high mass loss years. On the 100 survey line (Figure 1), which covers an elevation range of 329 m to 1,817 m, $\dot{b}_{insitu}$ averaged −1.2 m w.e. a^{-1} between 2006 and 2014. If only those years when >80% of all stakes were found are included in the calculation, the average $\dot{b}_{insitu}$ is then −1.4 m w.e. a^{-1}. On a year-to-year basis, $\dot{b}_{insitu}$ varied between −1.7 m w.e. a^{-1} (e.g., 2012–2013) and −0.3 m w.e. a^{-1} (e.g., 2013–2014). Maximum ice thicknesses on PIC are >700 m at 1,500 m a.s.l., ~3 km north of stake P105 (see Figure 1; Weber & Andrieux, 1970; Weber & Cooper, 1993), and a borehole drilled near the summit in 1995 (1,860 m a.s.l.) reached bedrock at a depth of ~334 m (Fisher et al., 1998). More recent measurements by a NASA airborne radar in 2013 confirm a maximum thickness of 880 m, ~5.5 km northwest of stake P106 (Shi et al., 2010).

Spaceborne passive microwave measurements have revealed that the average melt season length on PIC nearly doubled between 1979 and 2010 (Zdanowicz et al., 2012). Borehole and shallow core measurements from the ice cap's summit show that the firn density increased since the mid-1990s due to the formation of thick refrozen meltwater layers, which now account for 70–100% of annual accumulation. As a result of deep meltwater percolation, firn temperatures at 10 m depth rose by ~10°C between the mid-1990s and 2011 (Zdanowicz et al., 2012).

3. Data and Methods

3.1. Surface Elevation Change From Laser Altimetry

In spring 2005, 2013, and 2014, repeat airborne altimetry measurements were performed over PIC by NASA prior to the start of the ablation season (Figure 1). The 11 May 2005 mission used NASA's ATM sensor, which

has a swath width of ~140 m, a 1–3-m footprint for each laser shot, a ground spacing of 2–5 m, and nominal vertical accuracy of <0.2 m for a typical flight altitude of 500 m above the ice cap surface (Krabill et al., 1995). Since 2009, the ATM has been used in NASA's Operation IceBridge. The altimetry data on 12 April 2013 and 23 April 2014 were collected with a swath width of ~230 m, measurement density of ~1 per 10 m^2, a footprint of ~0.5 m, and a nominal vertical accuracy <0.1 m (Krabill, 2013).

We used the ATM L1B elevation data set, in which each altimetry surface elevation corresponds to one raw laser pulse (https://nsidc.org/icebridge/portal/map, last accessed 26 June 2019). A line of best fit, composed of points at 10-m spacing, was manually drawn along the flight ground track direction through the original 2005, 2013, and 2014 altimetry L1B data in ESRI ArcMap 10.1. At every 10 m along our line of best fit, the nearest altimetry point measurement was used to extract the surface elevation. Elevations between 2005 and 2013 were then subtracted to obtain the changes in elevation over time (*dh/dt*) along each track. Likewise, elevations between 2013 and 2014 were subtracted to obtain *dh/dt*. Points >10 m apart or outliers with *dh/dt* values equal to or greater than twice the maximum annual accumulation or ablation measured in situ (>= 3 or <= −8 m a^{-1}, respectively) were excluded from the analysis. Points with *dh/dt* values outside the 99.99% confidence interval (>5 standard deviations) about the altimetry data mean were also excluded. A manual check was then completed to remove anomalous points in areas of high relief, outside the ice cap, or where patterns were physically implausible (e.g., a change in *dh/dt* of 3 m a^{-1} or more between adjacent data points). In total, 2,853 points (8% of the total) were removed by applying these criteria. The accuracy of the airborne altimetry data are presented in supporting information S1. The ice cap extent was manually delineated from late summer 2014 Landsat 8 images (Schaffer, 2019). All elevation changes were standardized to units of meters per year (m a^{-1}).

Surface elevations over parts of PIC were also measured by the Geoscience Laser Altimeter System (GLAS) on board ICESat in 2009, and airborne ATM altimetry measurements by NASA were performed in 2013 along the ICESat ground tracks. Together, these data were used to calculate *dh/dt* from 2009–2013. ICESat data were collected during two campaigns in 2009: spring (2E; 09 March 2009 to 11 April 2009) and fall (2F; 30 September 2009 to 11 October 2009). Elevations were derived using Laser 2 only, due to the failure of Laser 3. GLAS has a circular footprint with a diameter of ~70 m and an average along-track spacing of 172 m (Zwally et al., 2011). A vertical accuracy better than 0.05 m is possible under optimal conditions (Fricker et al., 2005). However, the accuracy worsens over sloping terrain to 0.14 m for 0–1° slopes and 0.86 m for 3–5° slopes (Brenner et al., 2007; Moholdt et al., 2010). The GLAS data were downloaded from the National Snow and Ice Data Center (http://nsidc.org/data/icesat/index.html, last accessed 22 January 2014; GLA06L1B global surface elevation data product, release R33) and processed using the methodology of Nilsson et al. (2015). Raw ICESat data were filtered using quality flags and rejection parameters included in the product release. Tracks with large offsets were removed from the data set, and ICESat elevations were converted to the WGS84 ellipsoid from the TOPEX/Poseidon ellipsoid. The average elevation of altimetry data within a 70-m radius of each ICESat point was used to calculate the difference between the 2009 ICESat and 2013 altimetry data.

3.2. In Situ Mass Balance and dGPS Measurements

Between 2006 and 2014, annual measurements of surface mass balance (SMB) on PIC were made on a fixed-date system (Cogley et al., 2011) at stakes along the three survey lines during spring (Lines 100, 200, and 300) and on Coronation Glacier during summer, totaling 140 measurements at elevations ranging from 71–1,822 m a.s.l. (Figure 1). Line 100 (20 stakes) was first surveyed in 2006, Lines 200 and 300 (seven and nine stakes) in 2008, and Coronation Glacier (six stakes) in 2011. Snow pits were dug each year to the depth of the last summer surface (~0.1–1.6 m) at most stake locations, and a known volume of snow or firn from each stratigraphic layer was weighed to determine the density. Ice lenses were assigned a density of 845 kg m^{-3}, based on the average ice lens density from PIC firn/ice cores drilled in 2010. Thirty-two of the stake measurements were within 250 m of the 2005–2013 ATM altimetry survey lines.

To evaluate rates of near-surface vertical motion ($(dh/dt)_{top}$) over PIC, we used dual frequency global positioning system (dGPS) measurements of cartesian coordinates (x,y,z) made at the top of mass balance stakes on Survey Lines 100, 200, and 300 in April each year from 2011 to 2014. A Trimble R7 dGPS receiver was used with a minimum 20-min occupation time per stake. While many more dGPS measurements were collected, only 13 made on the same stake in two consecutive years were used for this analysis. The dGPS data

were postprocessed using the Precise Point Positioning method provided by Natural Resources Canada (http://webapp.geod.nrcan.gc.ca/geod/tools-outils/ppp.php, last accessed 15 November, 2018). Based on 15 dGPS measurements from April 2013, the resulting accuracies were ±0.09 m horizontally and ±0.10 m vertically at the 95% confidence level.

3.3. Mass Change Inferred From Altimetry Data

Surface elevation changes (dh/dt) along repeat altimetry lines were extrapolated to the entire ice cap using least-squares linear regression of dh/dt against the 2013 altimetry elevation. The resulting equation was applied to each of 1,700,494 grid cells of the Canadian Digital Elevation Data DEM (CDED DEM) of PIC to obtain a raster of dh/dt values, using the ice cap extent from late summer 2014. The CDED DEM has a resolution of 3–12 arc seconds, which equates to an average grid cell size over PIC of 60.91 × 60.91 m. The firn or ice volume change for each grid cell was then calculated from dh/dt, and the results were summed and multiplied by the grid cell size to generate an estimate of the total volume change over the whole ice cap area of 6,316 km^2. This was converted to mass change by multiplying cells by the average density of ice determined from ice cores (900 kg m^{-3}) to obtain the mass change rate $\dot{b}$ (Gt a^{-1}) between consecutive altimetry flights. To assess the sensitivity of the calculations to the assumed density of the firn zone, we also calculated the $\dot{b}$ with a density of 800 kg m^{-3} for firn, based on the average density of a shallow core drilled from the summit of PIC in 2013 (see section 3.4).

The extrapolation described in the preceding paragraph assumes that measurements of glacier elevation change (dh/dt) are directly related to mass change, but in reality, dh/dt include the effects of $\dot{b}$ (i.e., rate of net surface mass loss or gain) as well as the vertical component of motion due to firn densification or to ice flow (surface lowering or raising, also referred to as submergence or emergence; Cogley et al., 2011). The contributions of these factors to dh/dt can be clarified by a special case of the continuity equation:

$$\frac{dh}{dt} = \frac{\dot{b}}{\rho} + \left(\frac{dh}{dt}\right)_{den} + \left(\frac{dh}{dt}\right)_{dyn}, \quad (1)$$

where ρ is the associated density, $(dh/dt)_{den}$ is the surface lowering due to densification, and $(dh/dt)_{dyn}$ is the surface lowering or raising due to ice motion.

Equation 1 assumes that over the time scale considered here (a few years to decades), internal and basal mass change, isostatic displacement, and deepening of the glacier bed by erosion are negligible. If $\dot{b}$ is calculated from dh/dt over an entire ice cap with zero net mass change, it is reasonable to assume that surface lowering and raising cancel out such that the final term in equation 1 can be ignored. However, for a specific point on a dynamic ice cap, the term $(dh/dt)_{dyn}$ must be included as surface lowering (raising) can result in significant downward (upward) glacier motion. The densification term $(dh/dt)_{den}$ is often ignored in addition to $(dh/dt)_{dyn}$, and dh/dt is then assumed to be equal to $\dot{b}$. However, studies of borehole cores indicate that the firn density has increased substantially on large ice caps in the CAA in recent decades, as a result of melting and internal refreezing of meltwater (Bezeau et al., 2013; Zdanowicz et al., 2012). Therefore, the effect of firn densification must be accounted for. In this study, we calculated dh/dt from altimetry data, estimated $(dh/dt)_{den}$ and $(dh/dt)_{dyn}$ from ice core and dGPS measurements, and then used these data to modify altimetry-derived dh/dt to isolate $\dot{b}$. Details are provided below, and results of each step are presented in section 4.

3.4. Effect of Firn Densification

To determine the change in ice cap surface elevation due to densification ($(dh/dt)_{den}$) in the firn zone, we used data from ice or firn cores collected in 1995, 2010, and 2013 near the summit of PIC (Figure 2). The 1995 and 2010 cores were drilled 3.6 km east of the summit automatic weather station (AWS; 1860 m a.s.l.; Figure 1). The 1995 core reached bedrock at a depth of 334 m, while the 2010 core was 23 m long (Zdanowicz et al., 2012). The 2013 core was 6.7 m long and drilled adjacent to the AWS at 1,813 m a.s.l. For each core, the length and mass of each section (~20–40 cm long) was measured, and densities were calculated. Firn-core stratigraphy was documented from visual observations and checked against the density estimates.

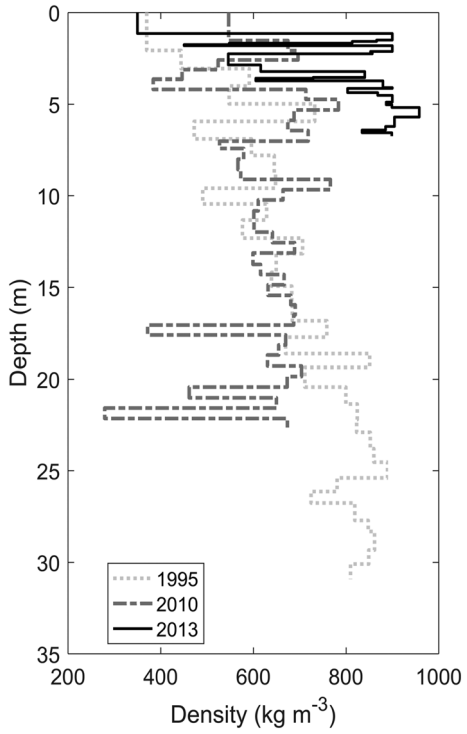

Figure 2. Density profile of ice cores from 1995, 2010, and 2013. The 2013 core was drilled adjacent to the summit AWS (Figure 1), while the two older cores were drilled 3.6 km east of the AWS.

The term $(dh/dt)_{den}$ was calculated from the change in thickness of near-surface firn layers down to a depth equivalent of 5 m w.e., which corresponds to the length of the shortest of the cores (6.7 m), drilled in 2013. A depth of 5 m w.e. is equivalent to ~17 years of accumulation based on the mean 1963–2010 accumulation rate of 0.39 m a^{-1} at the ice cap summit (Zdanowicz et al., 2012). The changes were calculated for 1995–2010 and 2010–2013, and the change for 2005–2013 was determined from a weighted average of both periods. For 1995–2010 and 2010–2013, the estimated values of $(dh/dt)_{den}$ were 0.08 and 0.53 m a^{-1}, respectively, and the weighted average for 2005–2013 was 0.25 m a^{-1} (Schaffer, 2019).

The calculations above only account for near-surface densification due to melting and refreezing (i.e., internal accumulation) and not for densification due to dry compaction below an equivalent depth of 5 m w.e. In situ refreezing of meltwater accounted for >80% of firn volume accumulation on PIC between 2000 and 2010, and this likely accounts for most near-surface densification (Zdanowicz et al., 2012). Ice core measurements from Devon Ice Cap in 2004 and 2012 also indicate that densification by refreezing of meltwater mostly occurs in the top 3–5 m of the firn zone (Bezeau et al., 2013).

Densification was assumed to occur only at elevations above the firn line on PIC, with no densification in the superimposed ice and glacier ice zones at lower elevations. To delineate the area where densification modifications to *dh/dt* apply, we used ground-penetrating radar (GPR) data acquired with a 500-MHz pulseEKKO PRO GPR along all three mass balance survey lines (Figure 1) in 2011, 2012, and 2013. The GPR was programmed with a time window of 1,000 ns (giving a penetration depth of ~80 m), and positions were recorded using an integrated single frequency GPS receiver or external Trimble R7 dGPS system. To determine the radar wave velocity, we used values of the dielectric constant inferred from the densities of shallow cores, following the methodology of Kovacs et al. (1995). The resulting radargrams were used to identify the areal extent of the firn zone in which firn layers are dominant to a depth of ~10 m, based on the presence of internal layering and high backscatter (Sylvestre et al., 2013). The GPR data interpretation was verified using shallow cores collected during spring 2011 to a depth of ~6 m below the glacier surface. These 2011 cores were not used for the firn densification calculations.

Synthetic aperture radar (SAR; C-Band) images were acquired with the Wide Swath ScanSAR instrument onboard Envisat on 19 October 2010. These images were then used to extrapolate the position of the firn-ice transition (outer boundary of the firn zone) identified in the GPR radargrams to all of PIC. The SAR imagery, with resolution of 150 × 150 m and a swath width of 405 km, was obtained through the European Space Agency Earth Observation Link (ESA EOLi) catalog. A scene acquired in a period of below-freezing conditions was selected to avoid complications in image interpretation due to surface melt. The SAR image was orthorectified, radiometrically corrected, and standardized to backscatter values (σ°, in dB) in PCI Geomatica. The resulting raster was imported into ArcGIS, and values along mass balance Survey Lines 100 and 300 were extracted for direct comparison with GPR results. The locations of the firn-ice transition (firn zone boundary) identified on the GPR radargrams were superimposed with the SAR data, and a threshold backscatter value of −5 dB was chosen to delineate the firn-ice transition (see supporting information S2). This compares well with Devon Ice Cap, where the firn-ice transition corresponds to backscatter thresholds of −5 to −7.8 dB on winter RADARSAT-1 images (Casey & Kelly, 2010).

Once the extent of the firn zone was delineated, the estimated mean $(dh/dt)_{den}$ value of 0.25 m a^{-1} over 2005–2013 was subtracted from all *dh/dt* data points within it. Since the firn densification rate likely varies across the firn zone, we also calculated modifications to *dh/dt* using two other scenarios. In the first ("minimum") scenario, $(dh/dt)_{den}$ was assumed to decrease from 0.25 m a^{-1} at the summit of PIC to zero at the outer limits of the firn zone. In the second ("maximum") scenario, $(dh/dt)_{den}$ was assumed to increase

Table 1
Annual Surface Height Changes (dh/dt) Measured at 13 dGPS Mass Balance Stakes Between 2011 and 2014 and the Corresponding Mean dh/dt for 2005–2013 Obtained by Altimetry (Alt.) Measurements Within the Same Elevation Band (±10 Vertical Meters)

Stake ID	Year (dGPS)	Elev. (dGPS) m a.s.l.	*dh/dt* (dGPS) m a^{-1}	*dh/dt* (Alt.) m a^{-1}	StDev (Alt.) m a^{-1}	*n* (Alt.)	*dh/dt* (dGPS) − *dh/dt* (Alt.) m
P000	2011–2012	1822	−0.76	−0.52	0.04	1322	−0.24
P101	2011–2012	1804	−0.77	−0.52	0.05	934	−0.25
P102	2011–2012	1722	−0.83	−0.48	0.10	762	−0.35
P103	2011–2012	1647	−0.35	−0.48	0.09	454	0.13
P104	2011–2012	1556	−0.90	−0.62	0.07	1165	−0.28
P105	2011–2012	1472	−0.45	−0.70	0.12	677	0.25
P105	2013–2014	1472	−0.55	−0.70	0.12	677	0.15
P110	2012–2013	1075	−0.25	−1.38	0.14	262	1.13
P112	2011–2012	943	−1.68	−1.37	0.11	383	−0.31
P113	2011–2012	880	−0.98	−1.43	0.10	123	0.44
P120	2011–2012	348	−2.51				
P202	2011–2012	1716	−0.58	0.48	0.10	826	−1.07
P203	2011–2012	1662	−0.55	−0.47	0.10	455	−0.08
Average			−0.72	−0.68	0.10	670	−0.04

Note. The standard deviation (StDev) and number (*n*) of altimetry points within each ±10 m elevation band and the difference between the two data sets are given for each stake location. The RMSE calculated for each stake is identical to the absolute values of the final column. Stakes within 250 m horizontal distance of the 2005–2013 altimetry lines are in bold.

downglacier, reaching a maximum of 0.425 m a^{-1} at the edge of the firn zone, based on data from a transect of ice cores across Devon Ice Cap (Bezeau et al., 2013). On Devon Ice Cap, the firn densification rate closest to the PIC firn zone boundary elevation (1,400–1,472 m) was 1.7 times higher than near the summit (1,800–1,900 m), so we multiplied the PIC $(dh/dt)_{den}$ rate of 0.25 m a^{-1} by 1.7 to obtain 0.425 m a^{-1}. Values of $(dh/dt)_{den}$ for all points within the firn zone were interpolated in ArcMap using the natural neighbor function and then subtracted from the corresponding elevation change values (dh/dt) at each point.

3.5. Effect of Ice Flow

The effect of ice flow (surface lowering or raising) on dh/dt was estimated from the interannual changes in the absolute height ($(dh/dt)_{top}$) of mass balance stakes measured by dGPS at 13 locations (Table 1; Schaffer, 2019). For each year, the $(dh/dt)_{top}$ at each stake was calculated by subtracting the change in height due to the downslope movement of the stake from the total height change measured since the previous year. The surface slope was derived from independent kinematic dGPS elevation measurements made over a horizontal distance of 200 m (100 m upglacier and downglacier) at each stake. The stakes were drilled 1–3 m into the near-surface firn (or ice) below the seasonal snowpack and assumed to remain frozen in place. The $(dh/dt)_{top}$ measurements were therefore presumed to be unaffected by changes in surface height due to mass loss (melt) or gain (accumulation), which would only affect the height of stakes relative to the snow/firn/ice surface. It was also assumed that the stakes did not melt downwards into the ice.

Measurements of $(dh/dt)_{top}$ for stakes in the firn zone may include contributions from both surface lowering ($(dh/dt)_{dyn}$) and densification ($(dh/dt)_{den}$). In these cases, the flow component ($(dh/dt)_{dyn}$) was obtained by subtracting from $(dh/dt)_{top}$ the estimated rate of firn densification below the bottom of the mass balance stakes (below 1.7 m). For depths greater than 1.7 m, this rate was estimated to be 0.21 m a^{-1} by comparing changes in the water-equivalent thickness of cores drilled within the firn zone of PIC in different years (see section 3.4). Outside the firn zone, $(dh/dt)_{dyn}$ was obtained directly from the $(dh/dt)_{top}$ measurements since there is no densification there. A linear regression of $(dh/dt)_{dyn}$ with respect to elevation was then used to extrapolate results across the entire ice cap.

3.6. Isolating the Rate of Surface Mass Loss or Gain From Geodetic Thickness Changes

Having separately estimated the components of dh/dt resulting from firn densification ($(dh/dt)_{den}$) within the firn zone and from ice flow ($(dh/dt)_{dyn}$) over the entire ice cap, we subtracted these components from the elevation change values (dh/dt) at each altimetry point to isolate the rate of surface mass change $\left(\dot{b}/p\right)$. These modified altimetry data sets were then extrapolated from the altimetry survey lines to the whole of

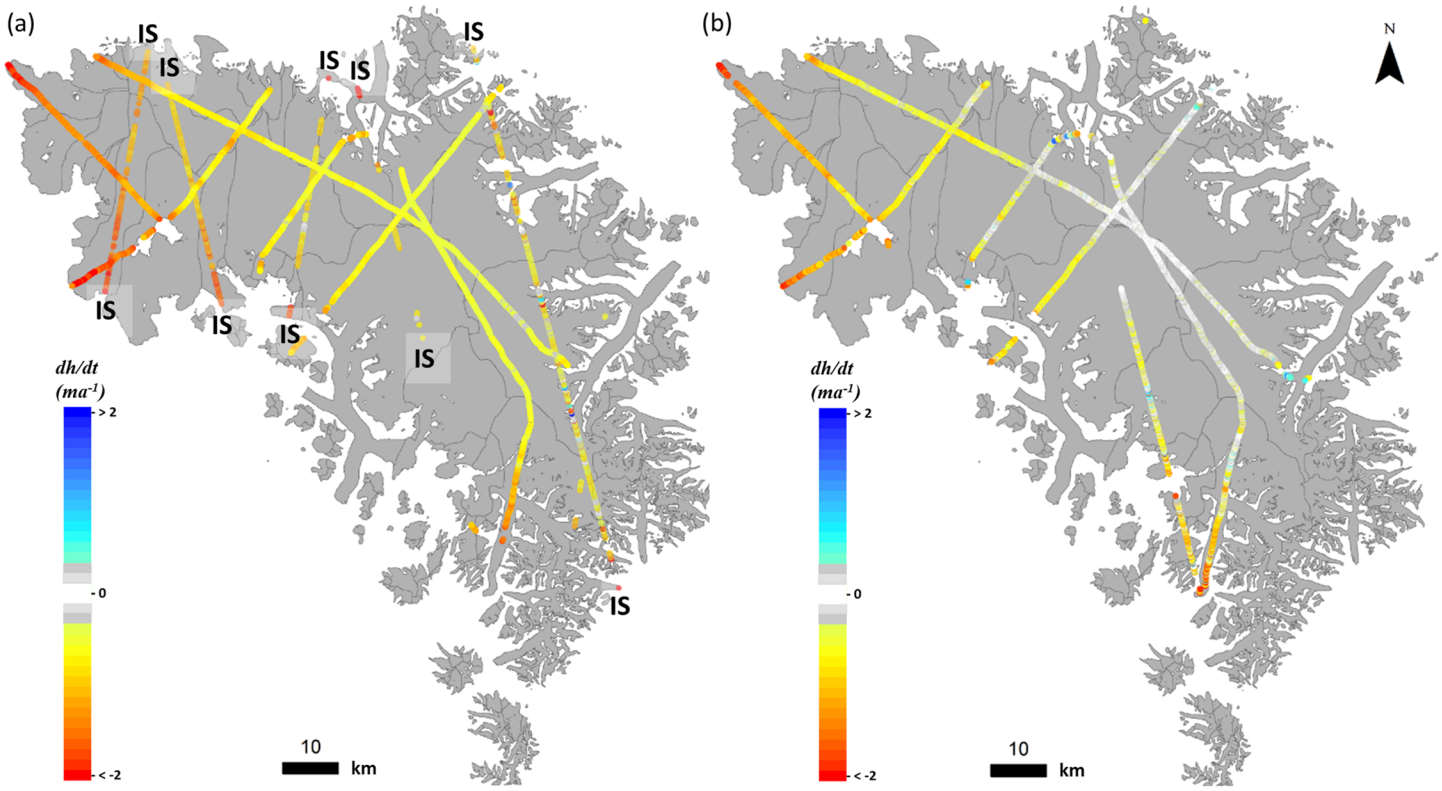

Figure 3. Surface elevation changes (*dh/dt*) on PIC measured by repeat laser altimetry between (a) 11 May 2005 and 23 April 2013 and (b) 12 April 2013 and 23 April 2014. In panel (a), *dh/dt* from 2009 ICESat and 2013 altimetry data on ICESat lines are also plotted, with ICESat lines lighter in color and labeled IS at both ends.

PIC using second-order polynomial regressions against surface elevation (see section 4.1). The resulting ice-cap-wide rasters, modified for firn densification and ice flow, were then multiplied by density to obtain the ice-cap-wide $\dot{b}$ following:

$$\dot{b}_{dens} = \left(\frac{dh}{dt} - \frac{dh_{den}}{dt}\right)\rho, \tag{2}$$

$$\dot{b}_{dyn} = \left(\frac{dh}{dt} - \frac{dh_{dyn}}{dt}\right)\rho. \tag{3}$$

In these equations, ρ is the assumed mean (bulk) density for the firn/ice mass, $\dot{b}_{dens}$ is $\dot{b}$ corrected for densification, and $\dot{b}_{dyn}$ is $\dot{b}$ corrected for ice flow, respectively. In applying the modifications (equations 2 and 3), we used two different bulk density schemes: (i) a uniform density of 900 kg m^{-3} applied to the whole ice cap and (ii) a density of 800 kg m^{-3} in the firn zone and 900 kg m^{-3} elsewhere. Scheme (i) assumes that only ice is lost, while Scheme (ii) allows for the loss of ice and firn.

4. Results

4.1. Altimetry Measurements

The *dh/dt* derived from altimetry measurements between May 2005 and April 2013 were negative over the entire ice cap, with thinning rates ranging from ~0.5 m a^{-1} in the summit area of PIC to >2 m a^{-1} at lower elevations on outlet glaciers and on the northwestern sector of the ice cap (Figure 3a; Schaffer, 2019). Between April 2013 and April 2014, *dh/dt* were less negative, with negligible changes in the summit area and thinning rates >2 m a^{-1} limited to small isolated areas at the lowest elevations (Figure 3b). The *dh/dt* measured by dGPS at 13 mass balance stakes between 2011 and 2014 measured in April each year (see

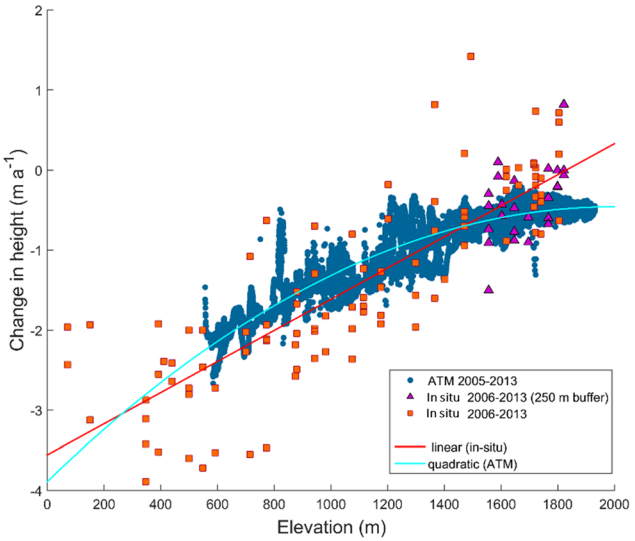

Statistic	In situ mass change	Altimetry 2005-2013
Regression type	Linear	Quadratic
Intercept	-3.56	-3.92
Coefficient (z)	0.0019	0.0035
Coefficient (z^2)		-8.77×10^{-7}
Adjusted R^2	0.72	0.88
p-value	< 0.001	< 0.001

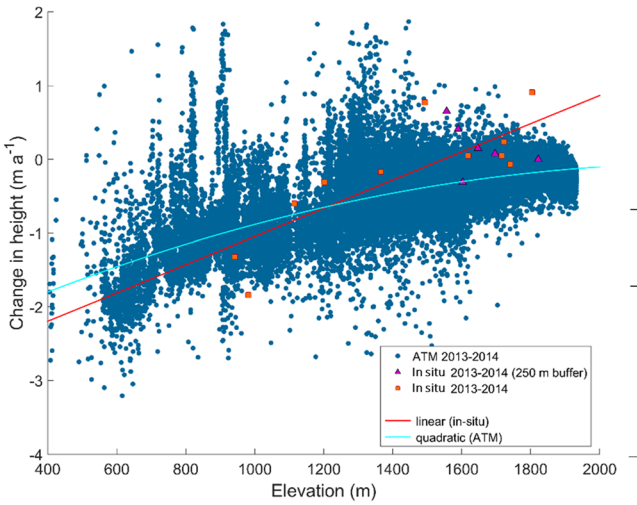

Statistic	In situ mass change	Altimetry 2013-2014
Regression type	Linear	Quadratic
Intercept	-2.96	-2.59
Coefficient (z)	0.0019	0.0022
Coefficient (z^2)		-4.65×10^{-7}
Adjusted R^2	0.58	0.46
p-value	< 0.001	< 0.001

Figure 4. Surface elevation changes over PIC based on unmodified altimetry measurements (*dh/dt*; blue dots) for (a) 2005–2013 and (b) 2013–2014, compared with in situ measurements of surface height changes due to mass change (red squares and purple triangles). The purple triangles are measurements within 250 m horizontally of the 2005–2013 altimetry flight ground tracks. Least squared best-fit lines are shown for the mass balance and altimetry data regressed against elevation (*z*). The regression coefficients are provided in tables adjacent to each plot.

section 3.5) were compared with the mean *dh/dt* over 2005–2013 derived from altimetry data acquired within a similar elevation band (± 10 m vertically; Table 1). The *dh/dt* dGPS data and airborne altimetry data are referenced to the ice cap surface, and the *dh/dt* measured therefore includes SMB, densification, and ice flow. The in situ dGPS data have been adjusted to remove vertical height changes due to the downslope movement of the mass balance stakes between measurements (see section 3.5; Schaffer, 2019). The mean difference between the *dh/dt* obtained by dGPS and by altimetry was 0.04 m, and the root mean square error (RMSE) was 0.39 m. The patterns of elevation change observed across PIC, with the largest thinning rates at low elevations on outlet glaciers and the northwestern sector of the ice cap, closely match the spatial distribution of *dh/dt* reported in previous studies (Abdalati et al., 2004; Gardner et al., 2012).

In Figure 4, we compare the *dh/dt* based on altimetry data with in situ measurements ($\dot{b}_{insitu}$), plotted as equivalent changes in surface height due to mass loss or gain (Schaffer, 2019). If the values of *dh/dt* are interpreted in terms of mass changes, they tend to overestimate ice losses at higher elevations (greater than ~1,500 m) and underestimate losses at lower elevations. This pattern holds true whether comparing the altimetry-derived *dh/dt* for 2005–2013 with measurements of $\dot{b}_{insitu}$ for 2006–2013 (Figure 4a) or for the

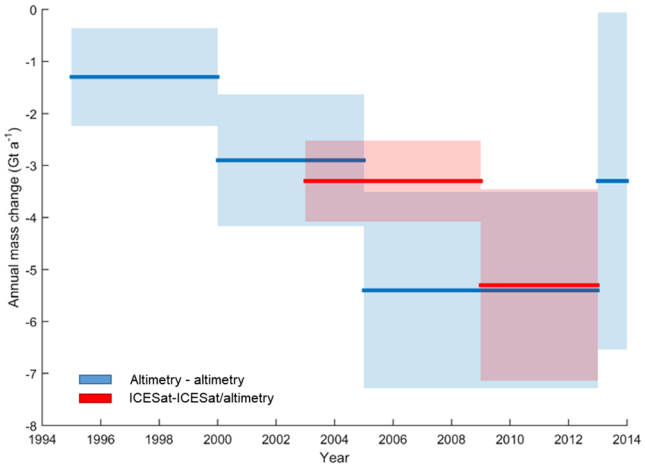

Figure 5. Estimates of mass change rates ($\dot{b}$) over PIC from 1995–2014 with 95% confidence intervals (shaded portion), based on altimetry data unmodified for densification. Estimates in blue were derived from airborne altimetry measurements only (1995–2000 and 2000–2005 from Gardner et al. (2012); 2005–2013 and 2013–2014 from this study). The 2003–2009 estimate in red is from spaceborne (ICESat) altimetry data only (Gardner et al., 2012), while the 2009–2013 estimate in red was derived in this study from a combination of ICESat (2009) and airborne altimetry data (2013).

2013–2014 altimetry dh/dt and $\dot{b}_{insitu}$ measurements (Figure 4b). The discrepancies are expected due to the effect of the vertical component of ice motion (Hagen et al., 2005), which increases the apparent (geodetic) ice loss rate at higher elevations due to surface lowering and lessens it at lower elevations due to surface raising.

In order to extrapolate the observed dh/dt on altimetry survey lines to the whole of PIC, different linear and polynomial models were least-square fitted to the unmodified dh/dt against elevation (Figure 4). A second-order polynomial (i.e., quadratic) model gave the best fit for the 2005–2013 altimetry data (adjusted $R^2 = 0.88$). The fit was poorer for the 2013–2014 data (adjusted $R^2 = 0.46$) owing to the larger variability of dh/dt values for any given elevation band in a single year (Figure 4), which tend to average out over multiple years. All regressions for dh/dt against elevation were statistically significant, as were the regression coefficients (p values < 0.001).

The quadratic model in Figure 4 used for extrapolating dh/dt data in space was derived from all ATM altimetry data points ($R^2 = 0.88$). We also divided the data into four groups (NW, NE, SW, and SE quadrants of PIC) and then subsequently extrapolated dh/dt data using four quadratic models, but this approach did not improve the R^2 of the regressions ($R^2 \leq 0.78$) and so was not used (see supporting information S3).

4.2. Unmodified Rate of Surface Mass Change From Altimetry Data

Extrapolating the 2005–2013 dh/dt data to the whole ice cap using the quadratic relationship from Figure 4 and assuming a mean $\rho = 900$ kg m^{-3} without any modification for firn densification or ice flow yields a mean $\dot{b}$ of -5.4 ± 1.9 Gt a^{-1} between 2005 and 2013 (Figure 5). This is over four times the mass loss rate between 1995 and 2000 estimated by comparable methods (-1.3 ± 0.72 Gt a^{-1}; Gardner et al., 2012). The same calculation over 2013–2014 gives a $\dot{b}$ of -3.3 ± 1.5 Gt a^{-1} (Figure 5). This figure is less negative than the mean for 2005–2013 because the geodetic year 2013–2014 corresponds to one of the least negative mass balance years (greater than -1.0 m w.e. a^{-1} on average along the 100 line for the mass balance year 2012–2013, measured in April 2013–2014) over the past decade (Gray et al., 2015; Harig & Simons, 2016). Comparison of 2005–2013 altimetry dh/dt data with 2009–2013 ICESat/altimetry dh/dt data reveals very similar spatial elevation change patterns at and near crossover points (Figure 3; Schaffer, 2019). Extrapolating the 2009–2013 ICESat data yields a $\dot{b}$ of -5.3 ± 1.8 Gt a^{-1}, which is identical, within error, to the figure computed from the 2005–2013 altimetry data (Figure 5).

Changes in melt and/or internal accumulation over the study period can be independently verified by comparing shallow (~6 m) cores collected adjacent to the AWS in the summit region of PIC in 2011 and 2013. Using the methodology of Zdanowicz et al. (2012), we estimated that the volumetric percentage of refrozen meltwater in near-surface firn at the summit of PIC, which results from summer melt, increased from 46% to 79% between 2011 and 2013 (includes the summers of 2011 and 2012). This is consistent with the elevation loss between 2005 and 2013 (includes the summers of 2005 and 2012) observed in the altimetry data.

4.3. Ice Flow Component of Surface Elevation Change

The estimated contribution of the ice flow ($(dh/dt)_{dyn}$) to the observed dh/dt over PIC is, as expected, positive in the lower parts of the ice cap (surface raising) and becomes increasingly negative (surface lowering) at higher elevations (Figure 6a). The pattern of $\dot{b}_{insitu}$ over PIC is opposite, with negative values at lower elevations and positive values at higher elevations, but the magnitude of variations differs from $(dh/dt)_{dyn}$. At the lowest elevation (348 m a.s.l.), $(dh/dt)_{dyn}$ is ~0.98 m a^{-1} while $\dot{b}_{insitu}$ is approximately -3.5 m a^{-1} or >3.5 times $(dh/dt)_{dyn}$. Moving upglacier the deviation decreases with $\dot{b}_{insitu}$ 3.2 times greater than $(dh/dt)_{dyn}$ at ~910 m a.s.l. and roughly in balance at the current ELA of ~1,646 m a.s.l. ($(dh/dt)_{dyn} = 0.15$ m a^{-1}, $\dot{b}_{insitu}$

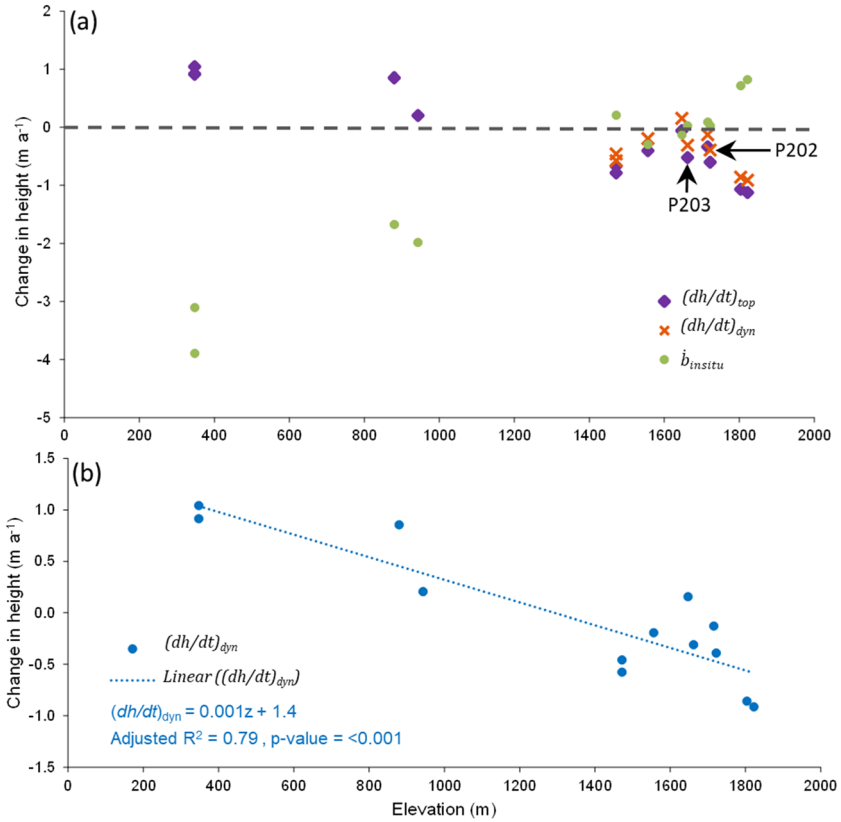

Figure 6. (a) $(dh/dt)_{top}$ is the measured interannual change in stake height measured by dGPS, $(dh/dt)_{dyn}$ is the component of $(dh/dt)_{top}$ due to dynamic ice surface lowering after firn densification has been accounted for, and $\dot{b}_{insitu}$ is the mass change data from the corresponding stake locations (all stakes are on Line 100, except for P202 and P203) plotted as changes in surface height. Outside the firn zone, $(dh/dt)_{top} = (dh/dt)_{dyn}$ since no firn densification occurs. (b) Least-square regression of $(dh/dt)_{dyn}$ against elevation with best fit linear regression line.

$= -0.13$ m a^{-1}). The transition between surface lowering and raising occurs between ~1,000 and 1,400-m elevation (Figure 6a).

Point estimates of $(dh/dt)_{dyn}$ were extrapolated across PIC using linear regression against elevation (Figure 6b). When summed over the entire ice cap, $(dh/dt)_{dyn}$ equals -0.01 m a^{-1}, which is within the

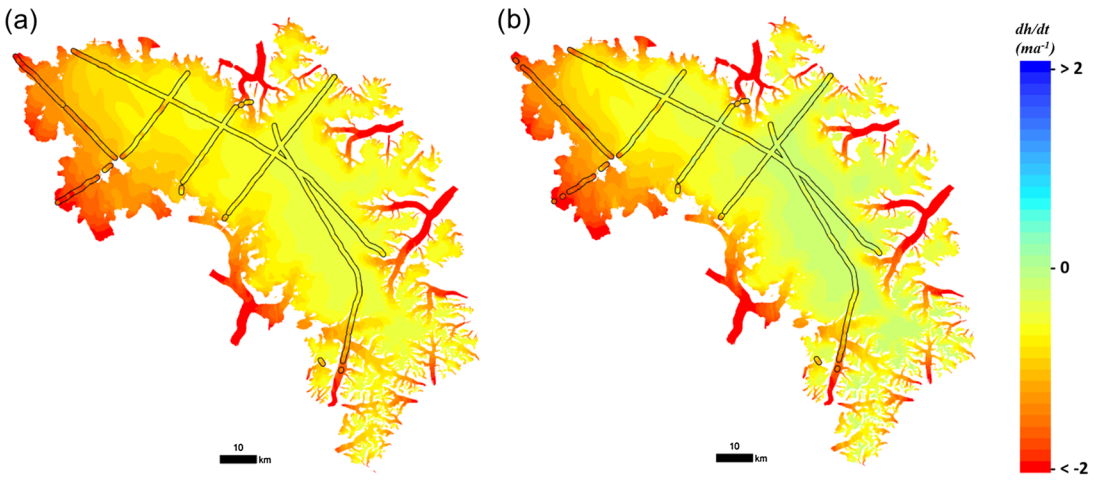

Figure 7. (a) Changes in surface elevation (dh/dt) across PIC between 2005 and 2013 extrapolated from altimetry data (plotted inside black buffer). (b) The same data, after modification for firn densification (constant densification scenario).

Table 2
Least Squared Best-Fit Line Regression Coefficients and Statistics for the Constant, Minimum, and Maximum Density Scenarios

Statistic Regression type	Constant Quadratic	Minimum Quadratic	Maximum Quadratic
Intercept	−4.28	−3.75	−4.77
Coefficient (z)	0.0040	0.0031	0.0048
Coefficient (z^2)	-9.76×10^{-7}	-6.99×10^{-7}	-1.26×10^{-6}
R^2	0.89	0.90	0.86
p value	< 0.001	< 0.001	< 0.001

uncertainty of the dGPS measurements (±0.1 m a^{-1}). The imbalance in $(dh/dt)_{dyn}$ could therefore be explained by uncertainties in the dGPS measurements and/or the interpolation. We conclude that the effects of dynamic surface lowering and raising across the ice cap cancel out and therefore have a negligible effect on the net volume and mass changes inferred from altimetry. Accordingly, we did not modify ice-cap-wide *dh/dt* for ice flow, but only for the effect of firn densification, as described below.

4.4. Rate of Surface Mass Loss or Gain Modified for Densification

In Figure 7, we compare the extrapolated, ice-cap-wide *dh/dt* derived from altimetry measurements between 2005 and 2013, before (a) and after (b) applying the modification for firn densification described in sections 3.4, 3.6, and S2 (Schaffer, 2019). The linear regressions used to extrapolate *dh/dt* modified for densification are shown in Table 2. It is readily apparent that modifying for densification decreases the estimated mass losses in the firn zone. Multiplying the modified *dh/dt* raster by $\rho = 900$ kg m^{-3}, we obtain an ice-cap-wide $\dot{b}_{dens}$ of −4.6 Gt a^{-1} ($\rho = 900$ kg m^{-3}), which is 15% less than the value obtained from the unmodified *dh/dt* (Table 3). This is a substantial difference but still within the margin of error of ±1.9 Gt a^{-1} for the estimate based on the unmodified *dh/dt*. If the "minimum" and "maximum" firn densification scenarios are applied to correct the 2005–2013 *dh/dt* data, the mass loss rates are −5.2 Gt a^{-1} $(\dot{b}_{dens\_min})$ and − 4.2 Gt a^{-1} $(\dot{b}_{dens\_max})$, respectively, when applying $\rho = 900$ kg m^{-3}.

In addition to the altimetry data, we calculate the mass change from in situ measurements to provide a full range of possible estimates. The ice-cap-wide value of $\dot{b}_{insitu}$ was calculated by extrapolating the in situ measurements for 2006–2014 using a linear least squared best fit model (Figure 4). These mass loss estimates are less than the unmodified altimetry data (Table 3). The bias and RMSE between the in situ measurements and a quadratic fit through the 2005–2013 unmodified (*dh/dt*) data set are 0.08 and 0.73 m, respectively (Table 3). The modified altimetry ice-cap-wide values of $\dot{b}$ for the "constant" and "minimum" scenarios ($\dot{b}_{dens}$ and $\dot{b}_{dens\_min}$) are closer to the in situ estimate, both having a bias and RMSE of ±0.03 and 0.71 m, respectively (Schaffer, 2019). We have used all of the $\dot{b}_{insitu}$ stake data for this comparison, including the 2013–2014 measurement year. While the 2013–2014 $\dot{b}_{insitu}$ data does not overlap with the 2005–2013 (*dh/dt*) data set, air temperatures and precipitation at the AWS for this year are very similar to 2005–2006 (mean annual air temperature −17.8°C and −17.4°C, total precipitation 6.1 and 5.9 m for 2013–2014 and 2005–2006, respectively, derived from RACMO2.3 output; Noël et al., 2015), and it is likely that the mass change is similar. As there is no $\dot{b}_{insitu}$ data available for 2005–2006, we include $\dot{b}_{insitu}$ from 2013–2014 as a substitute. Altimetry data (*dh/dt*) modified for densification and in situ data are plotted against elevation data in Figure 8.

If a density value of 800 kg m^{-3} is used in the firn zone and 900 kg m^{-3} elsewhere on the ice cap, the resulting unmodified $\dot{b}$, $\dot{b}_{dens}$, $\dot{b}_{dens\_min}$, and $\dot{b}_{dens\_max}$ are −5.2, −4.5, −5.0, and −4.1 Gt a^{-1}, respectively (Table 3). The

Table 3
Total Surface Mass Loss Rates Over PIC (dM/dt) Calculated From Unmodified Altimetry (Alt.) and Modified (Alt_{cor}) 2005–2013 dh/dt and 2006–2014 $\dot{b}_{insitu}$ Data, Using Density Scenarios of 900 and 800 kg m^{-3} in the Firn Zone and 900 kg m^{-3} Elsewhere

Scenario	dM/dt ($\rho = 900$ kg m^{-3}) (Gt a^{-1})	Percentage (Alt_{cor}/Alt.)	dM/dt ($\rho = 800$ kg m^{-3}) (Gt a^{-1})	Percentage (Alt_{cor}/Alt.)	Bias (m)	RMSE (m)
$\dot{b}$	−5.4	—	−5.2	96.5	0.08	0.73
$\dot{b}_{dens}$	−4.6	85.2	−4.5	83.0	−0.03	0.71
$\dot{b}_{dens\_min}$	−5.2	96.1	−5.0	93.2	0.03	0.71
$\dot{b}_{dens\_max}$	−4.2	76.9	−4.1	75.2	−0.06	0.74
$\dot{b}_{insitu}$	−5.1	94.5	−5.0	92.4		

Note. The differences between the surface mass loss rates calculated from the unmodified $(\dot{b})$ and modified altimetry data are expressed as a percentage of the unmodified data. The bias and RMSE between the $\dot{b}_{insitu}$ measurements and a quadratic fit through the 2005–2013 (*dh/dt*) data sets are reported.

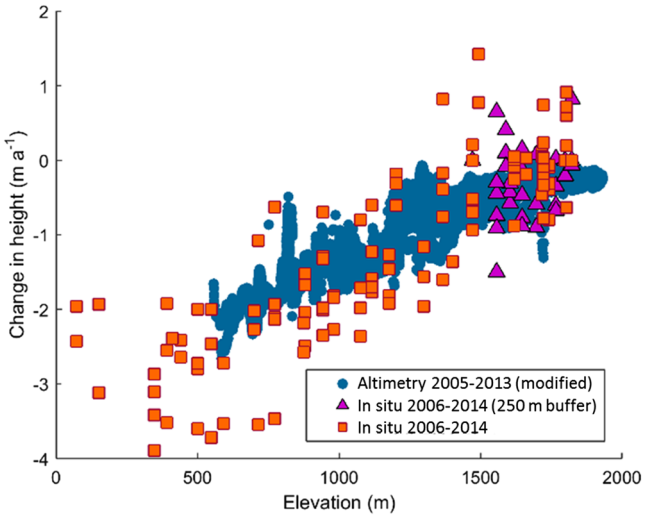

Figure 8. Altimetry elevation change from 2005–2013 (blue dots) modified for densification against elevation. In situ surface mass change measurements are included for reference with measurements within 250 m horizontally of the 2005–2013 NASA cloud shown as purple triangles.

surface mass loss for the unmodified *dh/dt* data is overestimated by 3.5% over PIC if volume loss is converted using 900 kg m^{-3} instead of 800 kg m^{-3} in the firn zone. When the *dh/dt* data set is modified for densification (constant density scenario), it is slightly less sensitive to a change in the assumed mean density of the firn zone, and the overestimation reduces to 2.2%.

5. Discussion

If repeat altimetry measurements are used to determine mass change for a specific point on the ice cap, the data should be modified for both vertical ice flow and densification. At any point on the surface, except for the dynamic equilibrium line, there will be a bias toward surface lowering or raising. On PIC, this can translate to an elevation change of up to ~1 m a^{-1} (Figure 6a). Densification within the firn zone can decrease the elevation by up to ~0.4 m a^{-1}.

Over the entire ice cap, repeat altimetry measurements should provide a good representation of $\dot{b}$ if (1) all elevation bands are represented and *dh/dt* values are obtained over a fairly uniform distribution of elevation bands; (2) the vertical component of ice flow ($(dh/dt)_{dyn}$) sums to zero; and (3) the firn density does not vary over time. We do not consider Point 1 above to be a significant factor in our measurements as the altimetry flight lines over PIC were generally well distributed with elevation (albeit with a slight bias toward higher elevations, with 53% of measurements at >1,500 m). However, if the altimetry data were not well distributed, it would likely be necessary to modify the altimetry points for flow since there would be a bias toward surface lowering or raising, depending on the spatial distribution of data. In relation to Point 2, the sum of ice-cap-wide $(dh/dt)_{dyn}$ of −0.01 m a^{-1} is within error limits of the dGPS measurements (± 0.1 m a^{-1}). The negative bias could also be due to compaction as the stake measurements ($(dh/dt)_{top}$) in the firn zone were modified for densification from melting and refreezing but not for dry compaction. Additional uncertainties exist given that the vast majority of point measurements used to determine $(dh/dt)_{dyn}$ are from one drainage basin and not evenly distributed across the ice cap. We conclude that $(dh/dt)_{dyn}$ sums to zero within error limits and that the ice flow component therefore has a negligible effect on the net volume and mass changes inferred from altimetry. For Point 3, it is clear that on PIC, the firn density is increasing over time (see section 3.4), and modifying the data for this decreases the mass loss estimates by ~4–21% (ρ = 800 kg m^{-3} within the firn zone; Table 3). We quote values with a density of 800 kg m^{-3} in the firn area as these are likely to be the most realistic based on field measurements. This decrease only applies to PIC, but comparable biases may apply elsewhere on Arctic glaciers where rapid densification changes have occurred. For example, the percentage of volume change attributed to firn densification for Greenland's glaciers and ice caps, estimated using a firn compaction model, was 15% and is within the range calculated for PIC (Bolch et al., 2013).

The inferred ice-cap-wide mass loss from $\dot{b}_{insitu}$ data (2006–2014) is 5% less than the unmodified altimetry data (ρ = 800 kg m^{-3} in the firn zone; Table 3). Other studies have also reported a more negative mass change inferred from elevation (geodetic) changes compared to the glaciological mass balance method (Beedle et al., 2014; Krimmel, 1999; Zemp et al., 2013). Many studies have used the mass change inferred from elevation change measurements to calibrate $\dot{b}_{insitu}$ data (e.g., Zemp et al., 2013). Our findings suggest that it is important to account for volume change due to densification prior to using these data if possible.

The positive densification rate calculated from ice cores on PIC is supported by a near-doubling of the volumetric percentage of refrozen meltwater in the top 6 m of firn near the summit between 2011–2013, coincident with an increase in the cumulative thickness of ice layers observed in GPR profiles along the Survey Line 100. Increased densification of firn over PIC has also been reported for the period 1995–2015 compared to 1958–1995 from regional climate model outputs (Noël et al., 2018). Similar changes in stratigraphy have been observed on other ice caps in the CAA and on Greenland, especially following the exceptional high

melt summer of 2012 (Bezeau et al., 2013; Gascon et al., 2013; MacFerrin et al., 2019; Machguth et al., 2016; Zdanowicz et al., 2012).

The surface lowering of 0.04 m a^{-1} due to densification in the top 1.25 m w.e. depth on PIC over the period 2005–2013 is comparable to the rates of 0.02–0.12 m a^{-1} calculated by Bezeau et al. (2013) between 2004–2012 for the summit of Devon Ice Cap. Our study highlights the importance of also accounting for densification at greater depths, given that densification in the top 1.25 m w.e. on PIC only accounts for 16% of the total surface lowering of 0.25 m a^{-1} that occurred in the top 5 m w.e.

A potential limitation in our method is the application of a densification rate for the whole firn zone based on measurements from a single location near the summit. Since it is likely that the firn densification rate varies across the firn zone, we also modified *dh/dt* using maximum and minimum densification schemes to provide a probable range of values for $\dot{b}$. Our maximum and minimum estimates produce ice cap $\dot{b}$ of −4.1 and −5.0 Gt a^{-1} (ρ = 800 kg m^{-3} in the firn zone), respectively, compared to that of −4.5 Gt a^{-1} for the constant density assumption. The constant and minimum densification scenarios have the lowest bias and RMSE when compared with $\dot{b}_{insitu}$ data (Table 3). Likewise, the estimated ice-cap-wide mass loss from $\dot{b}_{insitu}$ data of −5.0 Gt a^{-1} is closest to the minimum densification scenario. However, it is important to consider that the $\dot{b}_{insitu}$ data only accounts for mass loss or gain at the surface of the ice cap, while the altimetry data includes the surface, internal, and basal mass changes (Zemp et al., 2013). It is therefore possible that there is more densification occurring, but this is compensated for by positive internal and/or basal mass change. We also compared our mass loss calculations to those simulated by the regional climate model RACMO2.3 downscaled to 1 km over PIC (Noël et al., 2018). The simulated ice-cap-wide mass loss from RACMO2.3 between 2005 and 2013 is −4.0 Gt a^{-1}, which is closest to the maximum densification scenario. We conclude that the true mass loss is likely similar to the constant densification scenario, given that this scenario has a low RMSE compared to $\dot{b}_{insitu}$ data and is between the mass loss calculated from $\dot{b}_{insitu}$ and the RACMO2.3 model simulation. For comparison, we also calculate the mass loss by applying the recommended density of 850 kg m^{-3} (Huss, 2013), which incorporates densification, to the unmodified altimetry data for the entire ice cap. The resulting mass loss of 5.1 Gt a^{-1} is more negative than with the minimum densification scenario (ρ = 800 kg m^{-3} within the firn zone; Table 3). A bulk density of ~840 and ~ 750 kg m^{-3} applied ice-cap-wide would be required to obtain the same mass loss as the minimum and constant densification scenarios, respectively.

The method used to extrapolate *dh/dt* over the ice cap could be improved to better capture its spatial variability. While the chosen method of applying a polynomial fit based on elevation captures large-scale patterns, there are specific areas where the original *dh/dt* data differ from the extrapolated raster (Figure 7), such as within the northwestern lobe-like region. Incorporating other factors that may impact mass change such as slope, aspect, latitude, velocity, and solar radiation could provide ways to improve the extrapolation in the future.

Analysis of Envisat imagery shows that there are large areas of subsurface firn at elevations >400 vertical meters below the current ELA of 1,646 m (Figure S3). If the ice cap was in equilibrium with the climate, the firn-ice transition would be slightly upglacier of the ELA, at the boundary between the superimposed ice zone and wet snow zone. This discrepancy may be explained by the fourfold increase in mass loss since the mid-1990s and associated rapid upglacier migration of the ELA. There are few historical measurements of the ELA across PIC, but the study of Ward and Baird (1954) showed that it was at 1,380 m a.s.l. on Highway Glacier in 1953. The upward migration between 1953 and present day (~2010) was ~4.7 vertical meters per year. The current firn-ice transition at ~1,300 m a.s.l. is much closer to the 1953 ELA, suggesting a delayed response to the recent increase in melt rates. Similar results have been documented for Devon Ice Cap where the ELA migrated upglacier 188 m vertically between 2003 and 2006, but the firn-ice transition only migrated 24 m upglacier and was 140 m below the ELA in 2006 (Casey & Kelly, 2010). Given this scenario, we assume that firn is being lost and that assuming a bulk density of 800 kg m^{-3} when computing mass change within the firn zone is most realistic (Table 3).

The measured $\dot{b}_{insitu}$ is currently >3.5 times the magnitude of $(dh/dt)_{dyn}$ measured with a dGPS at low elevations. This difference is expected given that the ice cap is experiencing negative mass loss. The observed upward migration of the ELA would logically result in a reduced accumulation area and therefore surface

lowering zone, assuming that surface lowering is primarily driven by the amount of accumulated mass and that there is no significant lag in the ice flow response time compared to the SMB response time. A coincident decrease in the surface lowering zone area would likely result in a decreased surface raising rate per square meter in the ablation area, assuming that the surface lowering rate remains constant and that surface lowering and raising cancel at the ice-cap-wide scale. If there was a delay in the ice flow response time, the surface raising rate would be expected to remain unchanged for some time. Therefore, under negative mass change conditions with or without a lag, it is unlikely that the surface raising rate would compensate for the increased surface lowering (b), such that a difference between the two is expected under these conditions.

6. Conclusions

Mass loss on PIC has increased rapidly over the past two decades, from -1.3 ± 0.7 Gt a^{-1} between 1995 and 2000 (Abdalati et al., 2004) to -2.9 ± 1.1 Gt a^{-1} between 2000 and 2005 (Gardner et al., 2012) and -5.4 ± 1.9 Gt a^{-1} between 2005 and 2013 (Figure 5). This fourfold increase in surface mass loss rate since the period 1995–2000 is associated with increasingly positive temperature anomalies (Zdanowicz et al., 2012) and a rapid upglacier migration of the ELA, leading to large areas of subsurface firn at elevations >400 vertical meters below the current ELA. This shift in the ELA and observation that mass change is currently >3.5 times the magnitude of $(dh/dt)_{dyn}$ at low elevations illustrate that the ice cap is not in equilibrium and out of balance with the current climate. The accumulation area now only covers ~20% of the ice cap, and there has been a near-doubling of the volumetric percentage of refrozen meltwater in the top 6 m of firn near the summit from 2011–2013. This increase in mass loss on PIC is consistent with similar trends observed over other glaciers and ice caps on Baffin and Bylot Islands (Gardner et al., 2011; Gardner et al., 2012; Papasodoro et al., 2015, 2016).

Accounting for densification due to increased melt/refreezing on PIC results in a decrease in the inferred mass loss rate of ~13–15% from altimetry dh/dt measurements compared to unmodified data for the period 2005–2013, depending on the bulk density applied (ρ = 800 or 900 kg m^{-3} within the firn zone; Table 3). However, the lack of data on firn densification and vertical ice motion in earlier periods limits our ability to determine by how much earlier measurements should be modified. The modified dh/dt values are slightly less sensitive to the assumed density in the firn zone, used to convert volume to mass change, compared to the unmodified data. In order to reduce the uncertainty associated with the extrapolation of mass change and firn densification rates, we suggest that ice cores and a network of in situ mass change measurements be obtained over a range of elevations, with a spatial distribution representative of the ice cap in future studies.

This study represents the first ice-cap-wide evaluation of mass change distribution based on altimetry data modified for vertical motion in the Canadian Arctic and highlights the importance of accounting for firn densification when computing elevation change-derived mass changes. If $\dot{b}$ is computed at a point on the ice cap, the data should also be modified for flow. On PIC, surface lowering and raising can account for up to ~1 m a^{-1} of elevation change.

Acknowledgments

We thank Geological Survey of Canada staff (Alexander Chichagov and Mark Ednie), Parks Canada staff in Pangnirtung and Iqaluit, Alexandre Bevington, Patricia Payton and Charles Latour for their assistance with field work, Florent Dupont for supplying melt onset and end dates (passive microwave), Wesley Van Wychen for the original Matlab code used to process the altimetry data, Frances Delaney for providing the 2014 glacier outline, and the Department of Earth Sciences at Uppsala University for hosting N. Schaffer. We would also like to thank various data providers: National Snow and Ice Data Center (IceBridge altimetry data), GeoBase (CDED), European Space Agency (Envisat imagery), the U.S. Geological Survey (Landsat imagery), and the Geological Survey of Canada, Natural Resources Canada (PIC in situ data). This work was supported by funding from the Ontario Graduate Scholarship (OGS), Natural Sciences and Engineering Research Council of Canada (NSERC), Northern Scientific Training Program (NSTP), Canada Foundation for Innovation (CFI), Ontario Research Fund, Polar Continental Shelf Program (PCSP), ArcticNet Network of Centres of Excellence, and University of Ottawa. Support for David Burgess was provided through the Climate Change Geoscience Program, Earth Sciences Sector (Contribution No. 20160141), Natural Resources Canada. The data used in this study have been deposited in the Polar Data Catalogue (www.polardata.ca; Schaffer, 2019).

References

Abdalati, W., Krabill, W., Frederick, E., Manizade, S., Martin, C., Sonntag, J., et al. (2004). Elevation changes of ice caps in the Canadian Arctic Archipelago. *Journal of Geophysical Research*, *109*, F04007. 1–11. https://doi.org/10.1029/2003JF000045

Beedle, M. J., Menounos, B., & Wheate, R. (2014). An evaluation of mass-balance methods applied to Castle Creek Glacier, British Columbia, Canada. *Journal of Glaciology*, *60*(220), 262–276. https://doi.org/10.3189/2014JoG13J091

Berthier, E., Vincent, C., Magnússon, E., Gunnlaugsson, P., Pitte, P., le Meur, E., et al. (2014). Glacier topography and elevation changes derived from Pléiades sub-meter stereo images. *The Cryosphere*, *8*(6), 2275–2291. https://doi.org/10.5194/tc-8-2275-2014

Bezeau, P., Sharp, M., Burgess, D., & Gascon, G. (2013). Firn profile changes in response to extreme 21st-century melting at Devon Ice Cap, Nunavut, Canada. *Journal of Glaciology*, *59*(217), 981–991. https://doi.org/10.3189/2013JoG12J208

Bolch, T., Sandberg Sørensen, L., Simonsen, S. B., Mölg, N., MacHguth, H., Rastner, P., & Paul, F. (2013). Mass loss of Greenland's glaciers and ice caps 2003-2008 revealed from ICESat laser altimetry data. *Geophysical Research Letters*, *40*(5), 875–881. https://doi.org/10.1002/grl.50270

Box, J. E., Colgan, W. T., Wouters, B., Burgess, D. O., O'Neel, S., Thomson, L. I., & Mernild, S. H. (2018). Global sea-level contribution from Arctic land ice: 1971-2017. *Environmental Research Letters*, *13*(12). https://doi.org/10.1088/1748-9326/aaf2ed

Brenner, A. C., DiMarzio, J. P., & Zwally, H. J. (2007). Precision and accuracy of satellite radar and laser altimeter data over the continental ice sheets. *IEEE Transactions on Geoscience and Remote Sensing*, *45*(2), 321–331. https://doi.org/10.1109/TGRS.2006.887172

Casey, J. A., & Kelly, R. E. J. (2010). Estimating the equilibrium line of Devon Ice Cap, Nunavut, from RADARSAT-1 ScanSAR wide imagery. *Canadian Journal of Remote Sensing*, *36*(sup1), S41–S55. https://doi.org/10.5589/m10-013

Cogley, J. G., Hock, R., Rasmussen, L. A., Arendt, A. A., Bauder, A., Braithwaite, R. J., et al. (2011). *Glossary of glacier mass balance and related terms*, *IHP-VII Technical Documents in Hydrology No. 86*, IACS Contribution No. 2. Paris: UNESCO-IHP.

Cuffey, K. M. (2001). Interannual variability of elevation on the Greenland ice sheet: Effects of firm densification, and establishment of a multi-century benchmark. *Journal of Glaciology*, *47*(158), 369–377. https://doi.org/10.3189/172756501781832151

Fisher, D., Koerner, R. M., Bourgeois, J. C., Zielinski, G., Wake, C., Hammer, C. U., et al. (1998). Penny Ice Cap cores, Baffin Island,Canada, and the Wisconsinan Foxe Dome connection: Two states of Hudson Bay ice cover. *Science*, *279*(5351), 692–695. https://doi.org/10.1126/science.279.5351.692

Fricker, H. A., Borsa, A., Minster, B., Carabajal, C., Quinn, K., & Bills, B. (2005). Assessment of ICESat performance at the salar de Uyuni, Bolivia. *Geophysical Research Letters*, *32*, L21S06. https://doi.org/10.1029/2005GL023423

Gardner, A. S., Moholdt, G., Arendt, A., & Wouters, B. (2012). Accelerated contributions of Canada's Baffin and Bylot Island glaciers to sea level rise over the past half century. *The Cryosphere*, *6*(5), 1103–1125. https://doi.org/10.5194/tc-6-1103-2012

Gardner, A. S., Moholdt, G., Wouters, B., Wolken, G. J., Burgess, D. O., Sharp, M. J., et al. (2011). Sharply increased mass loss from glaciers and ice caps in the Canadian Arctic Archipelago. *Nature*, *473*(7347), 357–360. https://doi.org/10.1038/nature10089

Gardner, A. S., Moholdt, G., Cogley, J. G., Wouters, B., Arendt, A. A., Wahr, J., et al. (2013). A reconciled estimate of glacier contributions to sea level rise: 2003 to 2009. *Science (New York, N.Y.)*, *340*(6134), 852–857. https://doi.org/10.1126/science.1234532

Gascon, G., Sharp, M., Burgess, D., Bezeau, P., & Bush, A. B. G. (2013). Changes in accumulation-area firn stratigraphy and meltwater flow during a period of climate warming: Devon Ice Cap, Nunavut, Canada. *Journal of Geophysical Research: Earth Surface*, *118*, 2380–2391. https://doi.org/10.1002/2013JF002838

Gray, L., Burgess, D., Copland, L., Demuth, M. N., Dunse, T., Langley, K., & Schuler, T. V. (2015). CryoSat-2 delivers monthly and inter-annual surface elevation change for Arctic ice caps. *The Cryosphere*, *9*(5), 1895–1913. https://doi.org/10.5194/tc-9-1895-2015

Hagen, J. O., Eiken, T., Kohler, J., & Melvold, K. (2005). Geometry changes on Svalbard glaciers: Mass-balance or dynamic response? *Annals of Glaciology*, *42*(1), 255–261. https://doi.org/10.3189/172756405781812763

Harig, C., & Simons, F. J. (2016). Ice mass loss in Greenland, the Gulf of Alaska, and the Canadian archipelago: Seasonal cycles and decadal trends. *Geophysical Research Letters*, *43*(7), 3150–3159. https://doi.org/10.1002/2016GL067759

Huss, M. (2013). Density assumptions for converting geodetic glacier volume change to mass change. *The Cryosphere*, *7*(3), 877–887. https://doi.org/10.5194/tc-7-877-2013

Jacob, T., Wahr, J., Pfeffer, W. T., & Swenson, S. (2012). Recent contributions of glaciers and ice caps to sea level rise. *Nature*, *482*(7386), 514–518. https://doi.org/10.1038/nature10847

Kovacs, A., Gow, A. J., & Morey, R. M. (1995). The in-situ dielectric constant of polar firn revisited. *Cold Regions Science and Technology*, *23*(3), 245–256. https://doi.org/10.1016/0165-232X(94)00016-Q

Krabill, W. B. (2013). Icebridge ATM L1B elevation and return strength, version 2 (May 2005; April 2013; April 2014). Boulder, Colorado, USA: NASA National Snow and Ice Data Center Distributed Active Archive Center. https://doi.org/10.5067/19SIM5TXKPGT

Krabill, W. B., Thomas, R. H., Martin, C. F., Swift, R. N., & Frederick, E. B. (1995). Accuracy of airborne laser altimetry over the Greenland ice sheet. *International Journal of Remote Sensing*, *16*(7), 1211–1222. https://doi.org/10.1080/01431169508954472

Krimmel, R. M. (1999). Analysis of difference between direct and geodetic mass balance measurements at South Cascade Glacier, Washington. *Geografiska Annaler. Series A, Physical Geography*, *81*(4), 653–658. https://doi.org/10.1111/1468-0459.00093

Lenaerts, J. T., van Angelen, J., van den Broeke, M., Gardner, A., Wouters, B., & van Meijgaard, E. (2013). Irreversible mass loss of Canadian Arctic Archipelago glaciers. *Geophysical Research Letters*, *40*, 870–874. https://doi.org/10.1002/grl.50214

Li, J., Zwally, H. J., Cornejo, H., & Yi, D. (2003). Seasonal variation of snow-surface elevation in North Greenland as modeled and detected by satellite radar altimetry. *Annals of Glaciology*, *37*(1), 233–238. https://doi.org/10.3189/172756403781815889

Ligtenberg, S. R. M., Medley, B., van den Broeke, M. R., & Kuipers Munneke, P. (2015). Antarctic firn compaction rates from repeat-track airborne radar data: II. Firn model evaluation. *Annals of Glaciology*, *56*(70), 167–174. https://doi.org/10.3189/2015AoG70A204

Ligtenberg, S. R. M., Munneke, P. K., Noël, B. P. Y., & Van Den Broeke, M. R. (2018). Brief communication: Improved simulation of the present-day Greenland firn layer (1960-2016). *The Cryosphere*, *12*(5), 1643–1649. https://doi.org/10.5194/tc-12-1643-2018

MacFerrin, H., van Machguth, D. A., Charalampidis, C., Stevens, C. M., Heilig, A., Vandecrux, B., et al. (2019). Rapid expansion of Greenland's low-permeability ice slabs. *Nature*, *573*(7774), 403–407. https://doi.org/10.1038/s41586-019-1550-3

Machguth, H., MacFerrin, M., van As, D., Box, J. E., Charalampidis, C., Colgan, W., et al. (2016). Greenland meltwater storage in firn limited by near-surface ice formation. *Nature Climate Change*, *6*(4), 390–393. https://doi.org/10.1038/nclimate2899

Millan, R., Mouginot, J., & Rignot, E. (2017). Mass budget of the glaciers and ice caps of the Queen Elizabeth Islands, Canada, from 1991 to 2015. *Environmental Research Letters*, *12*(2). https://doi.org/10.1088/1748-9326/aa5b04

Moholdt, G., Nuth, C., Hagen, J., & Kohler, J. (2010). Recent elevation changes of Svalbard glaciers derived from ICESat laser altimetry. *Remote Sensing of Environment*, *114*(11), 2756–2767. https://doi.org/10.1016/j.rse.2010.06.008

Morris, E. M., & Wingham, D. J. (2014). Densification of polar snow: Measurements, modeling, and implications for altimetry. *Journal of Geophysical Research: Earth Surface*, *119*, 349–365. https://doi.org/10.1002/2013JF002898

Nilsson, J., Sorensen, L. S., Barletta, V. R., & Forsberg, R. (2015). Mass change of Arctic ice caps and glaciers: Implications of regionalizing elevation changes. *The Cryosphere*, *9*(1), 139–150. https://doi.org/10.5194/tc-9-139-2015

Noël, B., Van De Berg, W. J., Van Meijgaard, E., Kuipers Munneke, P., Van De Wal, R. S. W., & Van Den Broeke, M. R. (2015). Evaluation of the updated regional climate model RACMO2.3: Summer snowfall impact on the Greenland Ice Sheet. *The Cryosphere*, *9*(5), 1831–1844. https://doi.org/10.5194/tc-9-1831-2015

Noël, B., van de Berg, W. J., Lhermitte, S., Wouters, B., Schaffer, N., & van den Broeke, M. R. (2018). Six decades of glacial mass loss in the Canadian Arctic Archipelago. *Journal of Geophysical Research: Earth Surface*, *123*, 1430–1449. https://doi.org/10.1029/2017JF004304

Papasodoro, C., Berthier, E., Royer, A., Zdanowicz, C., & Langlois, A. (2015). Area, elevation and mass changes of the two southernmost ice caps of the Canadian Arctic Archipelago between 1952 and 2014. *The Cryosphere*, *9*(4), 1535–1550. https://doi.org/10.5194/tc-9-1535-2015

Papasodoro, C., Royer, A., Langlois, A., & Berthier, E. (2016). Potential of RADARSAT-2 stereo radargrammetry for the generation of glacier DEMs. *Journal of Glaciology*, *62*(233), 486–496. https://doi.org/10.1017/jog.2016.44

Schaffer, N. (2019). Revised estimates of recent mass loss rates for Penny Ice Cap, Baffin Island, based on elevation changes modified for firn densification. *Polar Data Catalogue*. https://doi.org/10.21963/13106

Schaffer, N., Copland, L., & Zdanowicz, C. (2017). Ice velocity changes on Penny Ice Cap, Baffin Island, since the 1950s. *Journal of Glaciology*, *63*(240), 716–730. https://doi.org/10.1017/jog.2017.40

Sharp, M., Burgess, D., Cogley, J., Ecclestone, M., Labine, C., & Wolken, G. J. (2011). Extreme melt on Canada's Arctic ice caps in the 21st century. *Geophysical Research Letters*, *38*, L11501. https://doi.org/10.1029/2011GL047381

Shepherd, A., Ivins, E., Geruo, A., Barletta, V. R., Bentley, M. J., Bettadpur, S., et al. (2012). A reconciled estimate of ice-sheet mass balance. *Science*, *338*(6111), 1183–1189. https://doi.org/10.1126/science.1228102

Shi, L., Allen, C. T., Ledford, J. R., Rodriguez-Morales, F., Blake, W. A., Panzer, B. G., et al. (2010). Multichannel coherent radar depth sounder for NASA operation ice bridge. *International Geoscience and Remote Sensing Symposium* (*IGARSS*), 1729–1732. https://doi.org/10.1109/IGARSS.2010.5649518

Sylvestre, T., Copland, L., Demuth, M. N., & Sharp, M. (2013). Spatial patterns of snow accumulation across Belcher Glacier, Devon Ice Cap, Nunavut, Canada. *Journal of Glaciology*, *59*(217), 874–882. https://doi.org/10.3189/2013JoG12J227

Thomson, L. I., Zemp, M., Copland, L., Cogley, J. G., & Ecclestone, M. A. (2017). Comparison of geodetic and glaciological mass budgets for White Glacier, Axel Heiberg Island, Canada. *Journal of Glaciology*, *63*(237), 55–66. https://doi.org/10.1017/jog.2016.112

Van Wychen, W., Copland, L., Burgess, D., Gray, L., & Schaffer, N. (2015). Glacier velocities and dynamic discharge from the ice masses of Baffin Island and Bylot Island, Nunavut, Canada. *Canadian Journal of Earth Sciences*, *52*(11), 980–989. https://doi.org/10.1139/cjes-2015-0087

Vincent, L. A., Zhang, X., Brown, R. D., Feng, Y., Mekis, E., Milewska, E. J., et al. (2015). Observed trends in Canada's climate and influence of low-frequency variability modes. *Journal of Climate*, *28*(11), 4545–4560. https://doi.org/10.1175/JCLI-D-14-00697.1

Ward, W. H., & Baird, P. D. (1954). Studies in glacier physics on the Penny Ice Cap, Baffin Island, 1953: Part I, A description of the Penny Ice Cap, its accumulation and ablation. *Journal of Glaciology*, *2*(15), 342–355. https://doi.org/10.1017/S0022143000025223

Weber, J. R., & Andrieux, P. (1970). Radar soundings on the Penny Ice Cap, Baffin Island. *Journal of Glaciology*, *9*(55), 49–54. https://doi.org/10.3198/1970JoG9-55-49-54

Weber, J. R., & Cooper, R. V. (1993). *Monitoring of elevation changes of the Penny Ice Cap, Baffin Island*. Ottawa: Geological Survey of Canada, Geophysics Division.

Zdanowicz, C., Smetny-Sowa, A., Fisher, D., Schaffer, N., Copland, L., Eley, J., & Dupont, F. (2012). Summer melt rates on Penny Ice Cap, Baffin Island: Past and recent trends and implications for regional climate. *Journal of Geophysical Research*, *117*, F02006. https://doi.org/10.1029/2011JF002248

Zemp, M., Thibert, E., Huss, M., Stumm, D., Rolstad Denby, C., Nuth, C., et al. (2013). Reanalysing glacier mass balance measurement series. *The Cryosphere*, *7*(4), 1227–1245. https://doi.org/10.5194/tc-7-1227-2013

Zwally, H. J., & Li, J. (2002). Seasonal and interannual variations of firn densification and ice-sheet surface elevation at the Greenland summit. *Journal of Glaciology*, *48*(161), 199–207. https://doi.org/10.3189/172756502781831403

Zwally, H. J., Schutz, R., Bentley, C., Bufton, J., Herring, T., Minster, B., et al. (2011). *GLAS/ICESat L1B Global Elevation Data V031, 20 February 2003 to 11 October 2009*. Boulder, CO: National Snow and Ice Data Center. Digital Media